Increasing the sonoporation efficiency of targeted polydisperse microbubble populations using chirp excitation

James McLaughlan, Nicola Ingram†, Peter R. Smith, Sevan Harput, P. Louise Coletta†, Stephen Evans‡, and Steven Freear, *Senior Member, IEEE*
Ultrasound Group, School of Electronic and Electrical Engineering, University of Leeds.
†Leeds Institute of Molecular Medicine, University of Leeds. ‡School of Physics and Astronomy, University of Leeds.

***Abstract*—The therapeutic use of microbubbles for targeted drug or gene delivery is a highly active area of research. Phospholipid-encapsulated microbubbles typically have a polydisperse size distribution over the 1-10 μm range and can be functionalised for molecular targeting as well as loaded with drug-carrying liposomes. Sonoporation through the generation of shear stress on the cell membrane by microbubble oscillations is one mechanism that results in pore formation in the cell membrane and can improve drug delivery. A microbubble oscillating at its resonant frequency would generate maximum shear stress on a membrane. However, due to the polydisperse nature of phospholipid microbubbles, a range of resonant frequencies would exist in a single population. In this study, the use of linear chirp excitations was compared with equivalent duration and acoustic pressure tone excitations when measuring the sonoporation efficiency of targeted-microbubbles on human colorectal cancer cells. A 3-7 MHz chirp had the greatest sonoporation efficiency of 26.9 $\pm$5.6 %, compared with 16.4 $\pm$1.1 % for the 1.32-3.08 MHz chirp. The equivalent 2.2 and 5 MHz tone excitations have efficiencies of 12.8 $\pm$2.1 % and 15.6 $\pm$1.1 %, respectively, which were all above the efficiency of 4.1 $\pm$3.1 % from the control exposure.**

***Index Terms*—Drug Delivery, Ultrasound Contrast Agents, Targeted Microbubbles, Sonoporation, Linear Frequency Modulation, Chirp.**

I. Introduction

GAS bubbles that have been stabilised with a thin shell material, typically phospholipids [1] or bio-compatible polymers [2], are routinely used as ultrasound contrast agents (UCA) as they are highly echogenic due to their compressible nature [3], [4]. Enhancing the contrast in echocardiography or improving signal-to-noise levels in Doppler imaging [5] are the main clinical uses for UCA. There is significant interest in the development of UCA, or microbubbles, as molecular imaging and/or therapeutic agents [6]–[10] since microbubbles can be conjugated with antibodies that target specific cell populations in the vasculature.

The therapeutic potential of microbubbles is predominantly as a delivery mechanism for drugs [11]–[14] or gene therapy vectors [15]–[19] that can be released through microbubble destruction by ultrasound pulses, or to enhance uptake of co-administered therapeutic agents. Additionally, mechanical damage associated with microbubble activity also has therapeutic potential [20]. Given the ubiquitous use of diagnostic ultrasound systems in the clinical environment, the infrastructure exists for targeted-microbubbles to be introduced for minimally invasive therapies [21].

The release of a therapeutic payload from a molecular-targeted microbubble would be achieved through its destruction from exposure to an ultrasound field. However, as microbubbles interact strongly with an ultrasonic field, the emitted/re-radiated pressure generated by microbubble oscillations could be used to enhance therapeutic efficiency though a process called sonoporation. Sonoporation is a technique that uses a combination of ultrasound and microbubbles to modify the permeability of a cell membrane [22], [23].

Although the exact mechanisms for sonoporation are unclear, it is thought that the production of shear stress on the cell surface by microbubble oscillations can result in an increased membrane permeability [24]. Additional sonoporation mechanisms such as the push and pulling behaviour resultant from the expansion and compression phase of microbubble oscillations near a membrane [12], [25], and acoustic microstreaming [26] are also thought to generate transient micropores through which a therapeutic agent can pass. Pores can also be generated by the formation of micro-jets by a microbubble undergoing non-spherical shape oscillations near a cell [27], which can result in non-viable cells and may not be useful for therapy in which the target cells must survive [28].

Phospholipid-encapsulated microbubbles typically have a polydisperse size distribution over the 1-10 μm range and can be functionalised for molecular targeting as well as loaded with drug-carrying liposomes [29], [30]. Microfluidic techniques for manufacturing monodisperse microbubble populations are in use, but the concentrations generated from these techniques are low when compared with available agents currently in clinical use [31]. Nevertheless, there are efforts to address this problem through generation *in situ* [32] or multiplexed devices [33].

The ultrasound frequencies used for sonoporation studies are typically below 2.5 MHz, with 1 MHz being a commonly used value [34]. A lower frequency would enable the microbubbles to be exposed at a higher mechanical index [35], [36], which might be needed in order to cause microbubble

James McLaughlan and Steven Freear are with the Ultrasound Group, School of Electronic and Electrical Engineering, University of Leeds, Leeds, LS2 9JT, UK. E-mail: j.r.mclaughlan@leeds.ac.uk, s.freear@leeds.ac.uk

destruction. A microbubble being excited by an ultrasound field that is at its resonant frequency would generate maximum shear stress on a cell membrane. However, phospholipid microbubbles, commercial or otherwise, have a polydisperse population and a range of resonant frequencies [37] would exist in a single population. Thus the use of a single frequency to excite the population may not be the most efficient method for generation of shear stress on cell membranes.

The use of linear frequency modulated chirps in diagnostic ultrasound imaging is a method for improving the signal-to-noise ratio and penetration depth of this imaging technique [38]–[40]. They have also been implemented to improve the contrast to tissue ratio when imaging with microbubbles [41], [42]. It has been proposed that due to the polydisperse nature of microbubble populations, if the frequency range of the chirp were to match those of the resonant frequency of the population, a greater acoustic response could be achieved [43].

The magnitude of shear stress incident on a cell from an oscillating microbubble is related to their separation distance [24], which can also affect the binding of a targeting ligand or antibody attached to the microbubble [44]. Primary radiation force [45] is used to manipulate microbubble populations [46] to assist in the molecular targeting of microbubbles [44], [47], [48], by minimising the distance between the cell and microbubble and thus maximising the incident shear stress on the cell. A secondary radiation force can be generated from the pressure gradients in the re-radiated ultrasonic field caused by microbubble oscillations. Two microbubbles that are excited either above or below their resonant frequency will result in an attractive force. This force will be negative if the microbubbles are oscillating out of phase [45]. The secondary radiation force can result in the formation of large aggregates of microbubbles [49]. It has been demonstrated theoretically that the use of a chirp with a polydisperse population will result in increased displacement of a microbubble population over an equivalent tone and thus could be beneficial for molecular targeting applications [50].

The aim of this study was to investigate whether the chirp excitation of polydisperse microbubble populations at low pressure amplitudes could be used to increase the sonoporation efficiency of cells, when compared to equivalent exposures at single frequencies.

II. Materials and Methods

A. Microbubble Manufacture and Characterisation

The phospholipids were prepared by mixing 19 μL of 1,2-dipalmitoyl-sn-glycero-3-phosphocholine (DPPC) and 6.5 μL of 1,2-distearoyl-sn-glycero-3-phosphoethanolamine-N-[biotinyl(polyethylene glycol)-2000] (ammonium salt) (DSPE-PEG2000 Biotin) (Avanti Polar Lipids, Alabaster, AL, USA), which were dissolved in stock solutions of chloroform with a concentration of 20 mg/ml. This resulted in a mol% of 92.3 and 7.7 %, respectively. After the chloroform had been evaporated using a vacuum desiccator, the lipids were re-suspended in a buffered saline solution of 99 % MilliQ water and 1 % (v/v) glycerine (Sigma-Aldrich, St. Louis, MO, USA) containing (w/v) 4 % NaCl in a single 1 mL vial using an ultrasound bath (U50, Ultrawave Ltd, Cardiff, UK). The vial containing the lipid solution was saturated with octafluoropropane (C_3F_8) gas and sealed. Microbubbles were generated by agitating this solution for 45 s in a CapMix mechanical shaker (3M ESPE, St. Paul, MN, USA) at a total concentration of $1.3\text{x}10^{10}$ $\pm 0.3\text{x}10^{10}$ microbubbles/ml. 97.5 μg of NeutrAvidin (A2666, Invitrogen Life Technologies, Paisley, UK), a biotin-binding protein, was added to 2 μg of anti-integrin $\alpha_v\beta_6$-biotinylated polyclonal antibody (bs-5791R-Biotin, Insight Biotechnology Ltd, Middlesex, UK) and incubated at room temperature for 20 minutes, which was then added to the microbubble solution and incubated at room temperature for a further 15 minutes to generate targeted microbubbles, using a one-pot approach. An immunofluorescent study was performed to confirm that the microbubbles were completely covered by fluorescent NeutrAvidin. A previous study [51] compared the sonoporation efficiency of targeted microbubbles and untargeted microbubbles, exposed to either a 2.2 MHz tone or 1.32-3.08 MHz chirp pulses. Untargeted microbubbles were manufactured by adding a biotinylated isotype control (Rabbit DA1E mAb IgG XP, New England Biolabs Ltd, Ipswich, MA, USA) to the microbubble solution.

In order to estimate the size distribution and concentration of the microbubbles, a 30 μl sample of 10x diluted solution was placed on a microscope slide, which had a chamber of fixed volume, and imaged using bright-field microscopy (Eclipse Ti, Nikon Instruments Inc., Melville, NY,USA) [52]. For small amplitude oscillations [53], the resonant frequency, ω_r, of an encapsulated microbubble that incorporates both the affects of stiffness and viscous damping of the shell [37] is given by

$$\begin{gathered}\omega_r^2 = \omega_0^2 - 2\beta^2 \\ \omega_0^2 = \frac{1}{\rho R_0^2}\left[3\gamma\left(P_0 + \frac{2\sigma}{R_0} + \frac{S_p}{R_0}\right) - \frac{2\sigma}{R_0} - \frac{3S_p}{R_0}\right] \\ \beta = \frac{1}{\rho R_0^2}\left[2\mu + \frac{S_f}{8\pi R_0}\right]\end{gathered} \tag{1}$$

where R_0 is the equilibrium radius of the microbubble (0.35-7.5 μm), ρ is the liquid density (998 kg/m^3), γ is the polytropic gas index (1.07), P_0 is the hydrostatic pressure (101 kPa), σ is the surface tension at the liquid gas interface (0.0728 N/m) and μ is the liquid viscosity (0.001 Pa.s). The values for shell stiffness, S_p, and viscosity, S_f, were 1 N/m and $0.05\text{x}10^{-6}$ kg/s, respectively and were chosen to be similar to a Definity™ microbubble [54]–[56] which have a similar shell composition and gas core to the microbubbles used in this study.

B. Ultrasound System

Two unfocused ultrasound transducers with a centre frequency of 2.2 or 5 MHz (V323 or V310, Element size

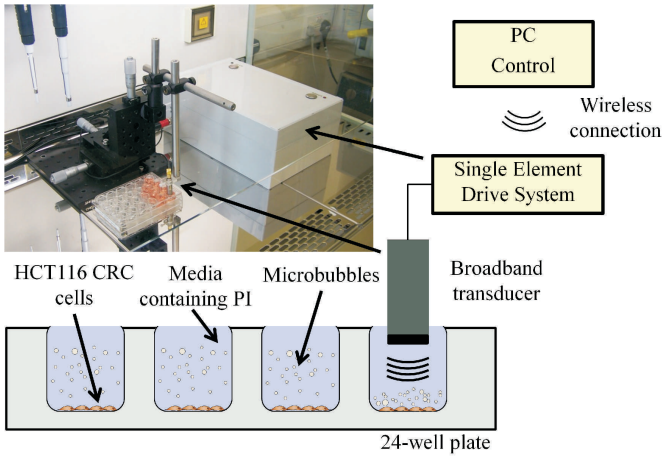

Fig. 1. A schematic showing the apparatus used for this sonoporation study. Cells were plated into a 24-well plate and microbubbles were added in the presence of Propidium Iodide, which were then exposed to ultrasound. The photograph inset shows the experimental apparatus within the bio-cabinet used in this study.

6.35 mm, -6dB bandwidth 79.9 %, Olympus NDT Inc, Waltham, MA, USA) were used to excite the microbubble population with either a tone or chirp pulse. A chirp with a -6dB bandwidth of 80 % was used for both transducers, which gave frequency ranges of 1.32-3.08 or 3-7 MHz. A 0.1 mm needle hydrophone (Precision Acoustics, Dorset, UK) was used to calibrate the output RMS pressure of both transducers, which was 110 kPa for all exposure parameters. For chirps, a pre-distorted drive signal was used to compensate for the transducer's frequency response to ensure uniform pressure amplitude across all frequencies.

A 10 μs duration burst with a pulse repetition frequency (PRF) of 1 kHz was used to expose the cell population for a total of 2 minutes. The transducers were mounted on a micrometer XYZ stage (PT3/M, Thorlabs Inc, Newton, NJ, USA) and positioned, in culture media, at 20 mm above the cell monolayer. Calibration of these transducers was performed at this distance to ensure that the ultrasound exposures were equivalent for each exposure type. Fig. 1 shows a schematic of the experimental setup used for this study. A high PRF was used to ensure that the primary radiation force exerted on the microbubble population was sufficient to push the microbubbles into contact with the cell monolayer at the bottom of the well, to aid binding. As all ultrasound exposures were performed in a plastic well a reflection from the bottom of the well was expected and had a reflection coefficient of σ_r = 0.25. These reflections affected the radiation force experienced by microbubbles distributed inside the media due to constructive and destructive interference of the long duration excitation waveform. However, the total net force was downward thus bringing the targeted microbubbles into contact with the cells. The targeted microbubbles that contributed towards sonoporation were located close to the cell monolayer and their proximity to the reflective boundary at the bottom of the well was at least an order of magnitude smaller than the shortest wavelength used in this study. Therefore it was assumed that the microbubbles were exposed with the incident pressure wave with minimal contribution from the reflected pressure wave.

The ultrasound transducer was driven by a custom-built single element drive system (Fig. 1), which was based on the Ultrasound Array Research Platform architecture reported previously [57]. The system is capable of driving transducer loads with excitation signal amplitudes up to $\pm$100 V using a commercially available integrated circuit (MAX4811, Maxim Integrated, San Jose CA, USA). This component operates in a switched-mode, generating square-wave 'pseudo-chirps'. A novel pulse width-modulation technique has been developed to provide output amplitude pressure control from the switched-mode system [58]. This technique allows arbitrary waveforms to be generated from the transducer, whilst maintaining the simplicity of switched-mode circuits. For this study, it was desirable to generate chirp sequences with an applied amplitude taper that counteracted the frequency characteristics of the transducer, thus equalising output pressure across the bandwidth of the signal. The amplitude function was derived from the inverse of the transducer's frequency response, and used in the design of each chirp excitation signal. Wireless control of the drive system via Bluetooth allowed for the entire experimental apparatus to be located within a bio-cabinet in order to reduce unnecessary cabling, minimise contamination risk and maintain sterility.

C. Cell Culture and Sonoporation Apparatus

Human mammalian HCT116 cells (American Type Culture Collection, Manassas, VA, USA) were used as a model colorectal cancer cell line, for the uptake of a fluorophore through sonoporation. The cells, with a passage number of 5, were seeded into each well of a 24-well plate with a density of 1.55x10^5 cells per well and cultured for 24 hours in RPMI 1640 media with 10 % Foetal Bovine Serum (Invitrogen Life Technologies, Paisley, UK), at 37 °C in a humidified atmosphere of 5 % $C0_2$ in air. The diameter of each well was 10 mm and the element of the ultrasound transducers was 6.25 mm. Cells were grown in monolayers up to a maximum overall confluency of 80 %. Prior to ultrasound exposures, the culture media in each well was replaced with 3 ml of media that contained the membrane impermeable fluorescent marker, Propidium Iodide (PI), (P3566, Invitrogen Life Technologies, Paisley, UK) at a concentration of 0.5 μM. Targeted microbubbles were added into each well at a concentration of 8x10^5 microbubbles/ml, except the wells used for control exposures. Sonoporation experiments were performed 24 h after seeding and thus it was estimated that there was approximately a microbubble to cell ratio of 3:1. The control measurements were ultrasound exposures of cell populations in the absence of microbubbles. Each exposure condition was repeated in three separate wells. Cells were then washed twice with fresh media.

To measure cell viability, a CellTracker Green stain (C2925, Invitrogen Life Technologies, Paisley, UK) was then added to each well at a concentration of 2 μM and left to incubate at 37°C for 45 minutes. This fluorescent green stain was used to indicate living viable cells since these reagents pass

freely through the membranes. However, once inside a viable cell, CellTracker Green is transformed into a cell-impermeant reaction product. After incubation, a final wash with fresh media was performed and then each well was imaged under both bright-field and fluorescence.

Immunofluorescence was performed on HCT116 cells in order to examine the presence of antigen (integrin $\alpha_v\beta_6$) used for molecular-targeting of the microbubbles in this study [59]. Glass cover slips were seeded with 50000 cells and left to culture for 48 hours and then fixed with 4 % paraformaldehyde in phosphate buffered saline (PBS) and followed by two washes with PBS. To minimise non-specific binding, blocking was performed using Antibody Diluent Reagent Solution (Invitrogen Life Technologies, Paisley, UK) for 1 minute before application of the primary antibody or isotype control (4096S, Rabbit DA1E mAb, New England Biolabs, MA, USA), which were each incubated for 1 hour at room temperature. The biotinylated antibody was applied at 1:50 dilution (concentration 1 mg/ml) and the isotype control at 1:100 (concentration 0.5 mg/ml). After washing, an AlexaFluor 488-conjugated secondary antibody (AlexaFluor 488 donkey anti-rabbit IgG, A-21206, Invitrogen Life Technologies, Paisley, UK), was incubated with the cells for 30 minutes in the dark at 1:300 dilution (concentration 2 mg/ml). After further washing with PBS the cover slips were mounted with Prolong Gold containing DAPI (Invitrogen Life Technologies, Paisley, UK). The fluorescent images were taken on a Zeiss Axio Imager Z1 microscope (Carl Zeiss Microscopy LLC, NY, USA) with AxioVision software, where the exposure times were kept constant between each acquisition. A test performed with the secondary antibody alone showed a similar staining to the isotype control.

A flow assay was performed in order to determine specific binding of microbubbles conjugated with the targeting antibody or an isotype control. HCT116 cells were seeded by plating 30 μl of 5x10^5 cells/ml onto the upper surface of a μ-Slide VI$^{0.4}$ (ibidi, Thistle Scientific, Glasgow, UK) and left to culture for 24 hours at 37 °C, in a humidified atmosphere of 5 % $C0_2$ in air. The cells were washed with PBS, then a solution containing 1x10^7 microbubbles/ml was flowed over the cells at a rate of 0.2 ml/minute for a total of 4 minutes using connecting tubing and a syringe driver (Aladdin AL-2000, World Precision Instruments, Sarasota, FL, USA). This flow corresponds to a shear rate of 40-50 s^{-1} and was chosen to maximise microbubble attachment without shearing off cells from the slide. In order to remove unbound microbubbles, PBS was flowed over the cells at a rate of 3.40 ml/minute for a total of 3 minutes. This flow corresponds to a shear rate of 600 s^{-1}, which is equivalent to the wall shear rate found at peripheral vessels in a glioma xenograft [60]. Five images of microbubbles bound to cells were acquired using a camera (C-7070, Olympus, Southend-on-Sea, UK) mounted onto an inverted light microscope (CKX41, 40x objective, Olympus, Southend-on-Sea, UK). The number of cells and the number of attached microbubbles was manually counted in each picture, with a mean number of cells per image of 122.

D. Analysis of Sonoporation Efficiency

Image sequences (bright-field and fluorescence) were acquired at five unique locations within each well, with a field of view of 205x153 μm. MatLab (Mathworks Inc, Natick, MA, USA) was used for image processing of both the bright-field and fluorescence images. A sequence of three images were taken; the bright-field images were used to identify the location and number of cells, and the average colour value was calculated under both red and green fluorescence. Threshold colour intensity values were identified from a well which had neither ultrasound nor microbubbles added to it, and only when both the respective average fluorescence values exceeded these values was a cell considered to be stained. PI is generally used to identify dead cells [61], [62], and this stain was used to avoid including dead or damaged cells.

An average of between 200-500 cells were imaged over the five unique locations in each well, which was then repeated three times for each exposure condition. Sonoporation efficiency was defined as the percentage of cells that had been stained with both red and green fluorescence. Cell viability was defined as the percentage of cells that were stained with CellTracker green, compared with the total number of cells imaged.

III. Results

Fig. 2(a) shows the measured size distribution for the microbubble population used in this study. The mean diameter and standard deviation for these microbubbles, based on measurements from five individual preparations, was 2.4 $\pm$1.0 μm. Fig. 2(b) shows the simulated range of resonant frequencies that was encompassed by the different sizes of this microbubble population. The two filled in areas under this curve show the range of resonant frequencies excited by either a 1.32-3.08 or 3-7 MHz chirp, which cover approximately 16.7 and 51.5 %, respectively, of this polydisperse population. However, the areas covered by tone excitations at 2.2 or 5 MHz excite approximately 1.5 and 1.3 % of the microbubble population at their resonance frequency, which is significantly lower than chirp excitation.

Fig. 3 shows the fluorescent staining of cells for the (a) integrin targeted and (b) isotype control antibodies. The bright green fluorescence staining in (a) shows the presence of the target antigen (integrin $\alpha_v\beta_6$) on the HCT116 cells that was used for microbubble targeting. A blue fluorescent stain was used to identify the cell nucleus. The fluorescent staining pattern shows the integrin is present in the membrane and cytoplasm and confirms the presence of the target antigen on these cells. This demonstrated that the antibody attached to the microbubbles was successfully targeted to the cell line used for this sonoporation study. In Fig. 3(b) faint green fluorescence is seen with the isotype control (exposure matched) indicating that a small degree of non-specific binding may occur with this antibody. Fig. 3(c) and (d) show two example images of microbubbles bound to cells for both the integrin and isotype control antibodies respectively. Fig. 3(e) shows that a

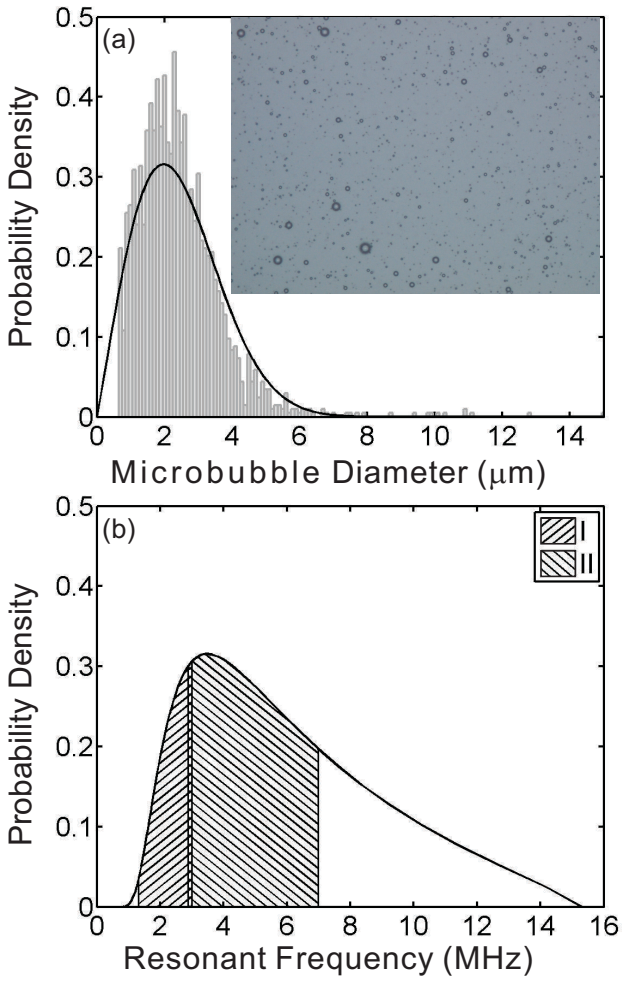

Fig. 2. (a) The population density of the microbubble population used in this study, which was normalised to the total number of microbubbles. The inset shows an example image of a microbubble population (b) The corresponding resonant frequency distribution of this polydisperse microbubble population. Hashed region (I) shows the population of microbubbles excited for a 1.32-3.08 MHz chirp and region (II) is for a 3-7 MHz chirp.

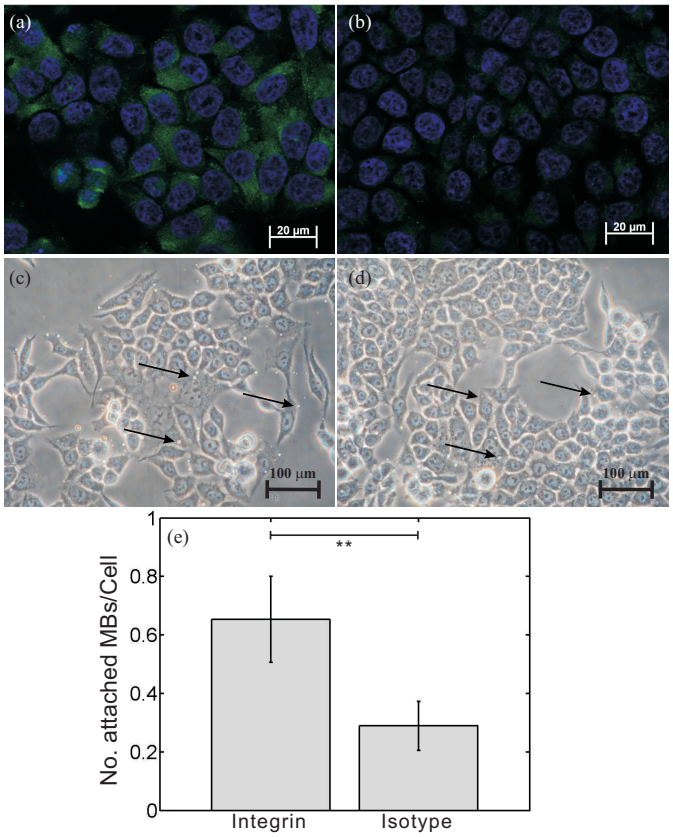

Fig. 3. Immunofluorescence images of HCT116 cells imaged under combined DAPI and FITC fluorescent filters for the (a) integrin antibody or (b) isotype control. Green fluorescence staining indicates the presence of the targeted antigen, where blue staining indicates cell nuclei. Microbubbles targeted with either (c) integrin $\alpha_v\beta_6$ or (d) isotype control antibody were flowed over HCT116 cells. In these images the microbubbles appear as white dots and are highlighted with arrows. (e) The number of attached microbubbles per cell for the integrin and isotype antibodies. $**$ shows statistical difference using a two-tailed Mann-Whitney U test where $p < 0.01$.

statistically significantly greater number of microbubbles binding to the HCT116 cells using integrin-targeted microbubbles compared to isotype-targeted microbubbles.

Fig. 4 shows the frequency spectrum of the four different exposure types measured using the needle hydrophone. Fig. 4(a) gives the frequency spectrum for the tone and chirp pulses generated using the 2.2 MHz transducer, where (b) is the frequency spectra generated with the 5 MHz transducer. The total power spectral density integrated over the 1-10 MHz range for each of these signals was approximately 5x10^4 dB/Hz^2, thus ensuring equivalent acoustic energy was delivered to the microbubble populations, irrespective of the exposure type.

Fig. 5, which has been reproduced from [51], shows the sonoporation efficiency for targeted and non-targeted microbubbles that have either been exposed to 2.25 MHz tone or 1.32-3.08 MHz chirp excitations. In addition, cells that had been exposed to a chirp excitation in the absence of microbubbles were used as a control. Although the overall sonoporation efficiency was below 21 %, targeted microbubbles that were exposed to a chirp excitation showed the highest sonoporation efficiency, with an efficiency of 20.5 $\pm$5.6 %. In addition, for both ultrasound exposure types, targeted microbubbles gave a higher efficiency when compared with non-targeted microbubbles.

Fig. 6 shows a mosaic of images taken under bright-field, red and green fluorescence for a single 205x153 μm location in each of the wells of diameter 10 mm, which were exposed to 110 kPa RMS pressure. The control exposure (Fig. 6a) was the only one of this sequence that was exposed without the presence of targeted-microbubbles. Fig. 6(b) and (c) were exposed using the lower frequency transducer with a 2.2 MHz tone and 1.32-3.08 MHz chirp, where (d) and (e) were the 5 MHz tone and 3-7 MHz exposures using the higher frequency transducer. The green stain indicates that these cell populations were viable. In this figure, cells stained both red and green were present only where microbubbles were introduced, indicative of sonoporation occurring in these cells. However, it is worth noting that even in the absence of microbubbles some viable cells had PI uptake. The cell viability for the control, 2.2 MHz tone and chirp, 5 MHz tone and chirp exposures was measured to be 98 $\pm$2.1 %, 98 $\pm$0.9 %, 98 $\pm$0.8 %, 96 $\pm$3.0 % and

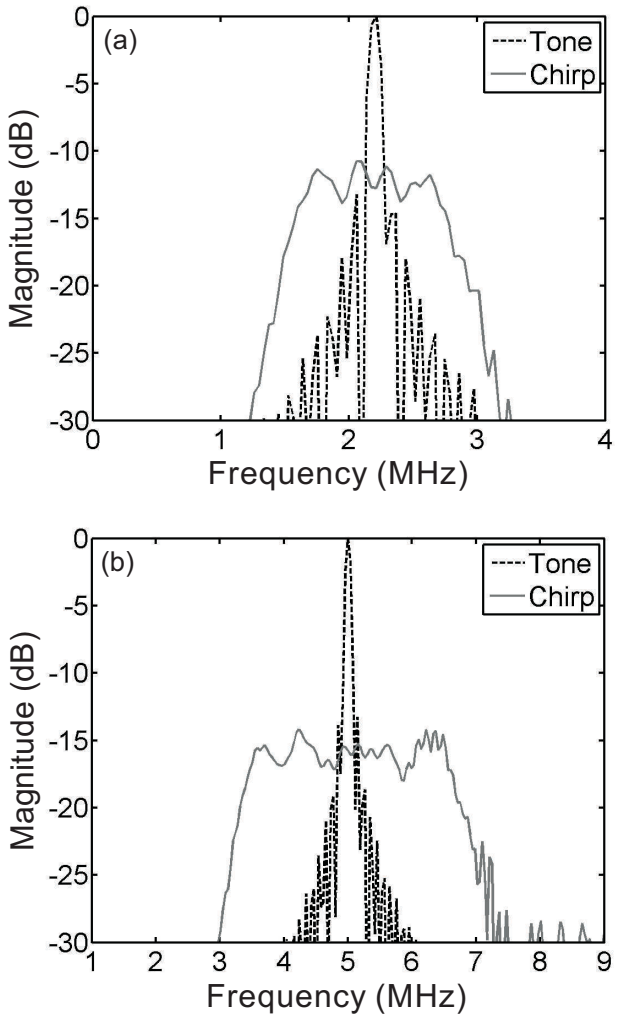

Fig. 4. (a) The measured frequency spectrum for the tone and chirp pulses centred at 2.2 MHz. (b) The corresponding frequency spectrum for the tone and chirp pulses centred at 5 MHz.

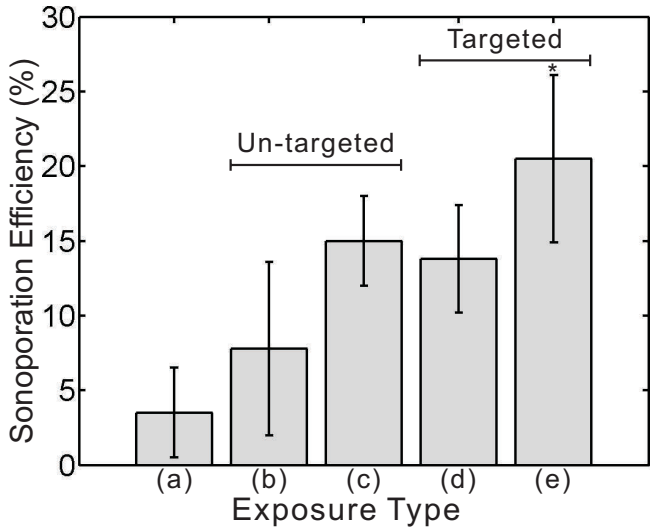

Fig. 5. The average sonoporation efficiency for targeted or un-targeted microbubbles exposed to (a) control, (b & d) 2.2 MHz tone, (c & e) 1.32-3.08 MHz chirp excitations. Error bars show the standard deviation of three repeat measurements. $*$ shows statistical difference from (a) the control measurement, with $p < 0.05$, using the Bonferroni's post-hoc test.

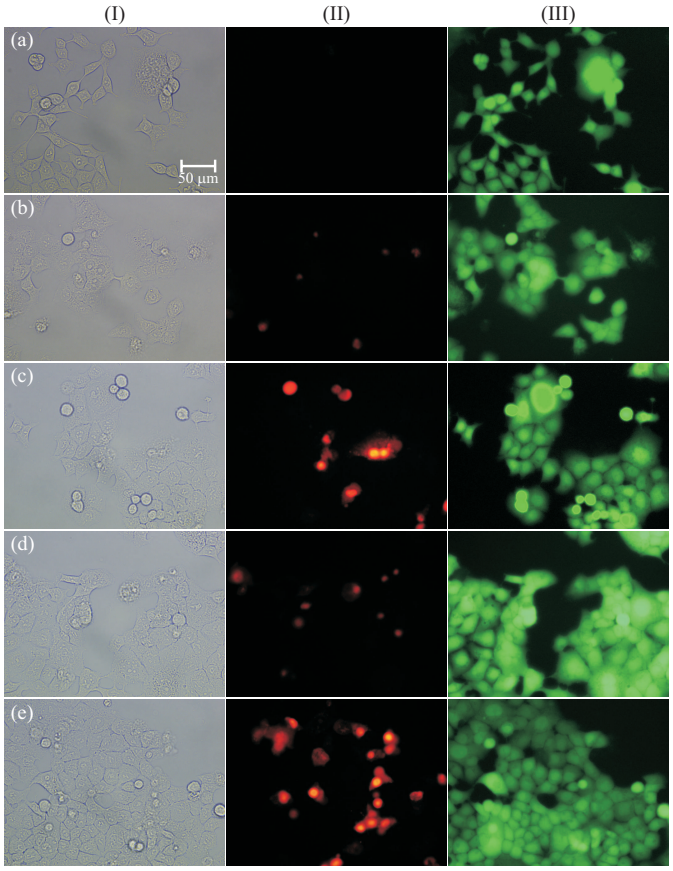

Fig. 6. A mosaic of (I) bright-field, (II) red and (III) green fluorescence images for the (a) control, (b) 2.2 MHz tone and (c) chirp, (d) 5 MHz tone and (e) chirp exposures.

96 $\pm$1.6 %, respectively.

Fig. 7 shows the sonoporation efficiency in HCT116 cells for targeted microbubbles that have been exposed to (b) 2.2 MHz tone, (c) 1.32-3.08 MHz chirp, (d) 5 MHz tone or (e) 3-7 MHz chirp excitations. Fig. 7(a) shows the sonoporation efficiency for the control exposure, comprised of cells exposed to a 3-7 MHz excitation in the absence of microbubbles. The high frequency chirp (Fig. 7e) showed the greatest sonoporation efficiency of 26.9 $\pm$5.6 %, compared with 16.4 $\pm$1.1 % for the lower frequency chirp. Similarly the 2.2 and 5 MHz tone excitations has efficiencies of 12.8 $\pm$2.1 % and 15.6 $\pm$1.1 %, respectively.

A sonoporation efficiency of 4.1 $\pm$3.1 % was achieved with the control exposure. A one-way analysis of variance test demonstrates that the means of the different exposure groups in Fig. 7 were significantly different with $p < 0.0001$. Further analysis using the Bonferroni's post-hoc test to compare each group with every other indicates that only the efficiency measured for 2.2 MHz tone excitations was not significantly different to the control measurements. Analysis also showed that the measured efficiency for the 3-7 MHz chirp exposure was significantly greater than the other exposure conditions.

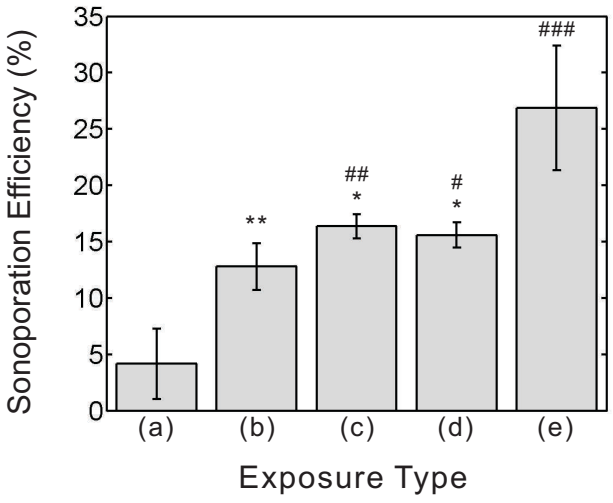

Fig. 7. The average sonoporation efficiency for targeted microbubbles exposed to (a) control, (b) 2.2 MHz tone, (c) 1.32-3.08 MHz chirp, (d) 5 MHz tone and (e) 3-7 MHz chirp excitations. Error bars show the standard deviation of three repeat measurements. ###, ## or # show statistical difference from (a) the control measurement, with $p < 0.001$, 0.01 or 0.05 respectively, using the Bonferroni's post-hoc test. $**$ or $*$ show statistical difference from (e) the 5 MHz chirp excitation, with $p < 0.01$ or 0.05.

IV. Discussion

The sonoporation efficiencies achieved in HCT116 cells for this study were between 12-27 % for all exposure conditions with targeted microbubbles. However, the use of targeted microbubbles exposed to a chirp excitation resulted in the greatest efficiency when compared with equivalent tone excitation. As shown in Fig. 7, the highest efficiency was generated by a chirp at 3-7 MHz followed by the 1.32-3.08 MHz chirp with 16.3 %. Cell viability was measured 45 minutes after exposure, whereas later time points may have shown greater cell death and thus affect the sonoporation efficiency is a limitation of this study. The reported sonoporation efficiency of 4.1 $\pm$3.1 % for the control measurements shows a very low uptake of PI into viable cells in the absence of microbubbles. It has been widely reported that ultrasound exposures alone are sufficient to result in uptake into the cell, but as greatly reduced levels when compared with ultrasound and microbubbles [19].

The resonant frequencies predicted by Eq. (1) for the size distribution of this specific microbubble population is shown in Fig. 2, which highlights that the higher frequency chirp would excite approximately 51.5 % of the population at resonance, compared with 16.7 % for the lower frequency chirp. The accuracy of this estimation could be improved by using measured shell parameters for this specific population. Furthermore, in this study a constant chirp rate was used, thus fixing the exposure duration at a specific frequency. A further increase in the sonoporation efficiency could possibly be achieved through the use of a non-linear chirp rate. This chirp rate would be defined by the measured resonant response of the polydisperse microbubble population used and would ensure that a greater population of microbubbles at a specific size would experience excitation at resonance for longer in an effort to maximise the shear stress generated on the cells. In addition, transducers with a broader bandwidth, such as capacitive micromachined ultrasonic transducers (CMUTs) [63] could be used to increase the population of microbubbles excited at resonance without the need to sacrifice output power. This would allow for higher acoustic pressures to be tested, which is a limitation of this study. The primary aim of this study was to compare tone and chirp excitations for the sonoporation of cancer cells and thus an exposure duration of 2 minutes was chosen, from a large variation of exposure times [34], to ensure adequate time for primary radiation force to bring the microbubbles into contact with the cells and for sonoporation to occur. However, this duration could be optimised by monitoring the acoustic backscatter from microbubbles so that exposures could last until the microbubble population has diminished, thus maximising the time for sonoporation to occur. Further optimisation could be achived through increasing the duration and PRF of the ultrasound exposure, but this could result in decreased cell viability [64].

Fig. 5 shows a the sonoporation efficiency of targeted and un-targeted microbubbles exposed to both tone and chirp pulses. In this example the targeted microbubbles exposed to a chirp excitation preformed than equivalent exposure without targeting. The magnitude of shear-stress experienced by a cell is dependent on the separation distance between the cell and microbubble [24]. Thus, bound microbubbles may show increased sonoporation efficiency due to being in close proximity to the cells for the duration of the ultrasound exposure when compared with free microbubbles.

As the microbubbles were introduced into the media and uniformly distributed, primary radiation force was used to bring them into contact with the cell populations to facilitate binding and sonoporation. However, secondary radiation force effects resultant from microbubble oscillations have been shown [65] to cause clusters of microbubbles around individual cells or have sufficient force to break molecular bonds [66]. This clustering effect due to secondary radiation force could have impacted the overall sonoporation efficiency in this study since the microbubble population is not evenly distributed over all of the cells, and could be restricted to individual locations on the cell. In a sonoporation study using targeted microbubbles to deliver PI into endothelial cells, Kooiman *et al*, [67] demonstrated that the location of attachment of targeted microbubbles did not affect the sonoporation of the cell, but also observed that sonoporation did not always occur with a microbubble located on a cell. A possible cause for this may have been due to driving microbubbles off-resonance with a 1 MHz tone excitation, as a polydisperse microbubble population was used [68]. This study demonstrated that a single targeted microbubble on a cell can result in sonoporation and thus the formation of microbubble aggregates on single cells would be an inefficient technique for drug delivery. However, this effect is increased through the experimental arrangement used in this study and may not be a significant problem *in vivo*.

An inverse filter based on the transducer's transfer function was used to pre-distort the electrical drive signal to ensure that the RMS pressure was kept constant at 110 kPa for each exposure parameter, and thus compensate for the

transducer's frequency response. In order to increase the spectral energy, the maximum peak pressure achievable with this system was limited when compared with the tone excitations. However, this technology has been implemented into an array system [58], which will be able to provide RMS pressures at higher amplitudes. Furthermore, the integration of pre-distorted chirp pulses into diagnostic ultrasound systems could provide a valuable tool in the clinical use of microbubbles for targeted drug delivery.

V. Conclusions

This study demonstrated that the use of chirp excitation of molecular-targeted polydisperse microbubble populations resulted in higher sonoporation efficiencies of cultured cell monolayers when compared with tone bursts of equivalent duration and RMS pressure. A 3-7 MHz pre-distorted chirp showed the greatest sonoporation efficiency of 26.9 $\pm$5.6 %, which might be further, improved through the use of non-linear chirp excitation.

Acknowledgment

This work was supported by EPSRC grant EP/I000623/1.

References

[1] M. Schneider, M. Arditi, M. Barrau, J. Brochot, A. Broillet, R. Ventrone, and F. Yan, "Br1: a new ultrasonographic contrast agent based on sulfur hexafluoride-filled microbubbles." *Invest Radiol*, vol. 30, no. 8, pp. 451–457, 1995.

[2] P. Narayan and M. A. Wheatley, "Preparation and characterization of hollow microcapsules for use as ultrasound contrast agents," *Polym Eng Sci*, vol. 39, no. 11, pp. 2242–2255, 1999.

[3] B. B. Goldberg, J.-B. Liu, and F. Forsberg, "Ultrasound contrast agents: A review," *Ultrasound in Medicine & Biology*, vol. 20, no. 4, pp. 319–333, 1994.

[4] D. Cosgrove, "Ultrasound contrast agents: An overview," *European Journal of Radiology*, vol. 60, no. 3, pp. 324–330, 2006.

[5] J. R. Lindner, "Microbubbles in medical imaging: current applications and future directions," *Nat Rev Drug Discov*, vol. 3, no. 6, pp. 527–533, 2004.

[6] A. L. Klibanov, "Microbubble contrast agents: Targeted ultrasound imaging and ultrasound-assisted drug-delivery applications," *Investigative Radiology*, vol. 41, no. 3, pp. 354–362, 2006.

[7] M. R. Bohmer, A. L. Klibanov, K. Tiemann, C. S. Hall, H. Gruell, and O. C. Steinbach, "Ultrasound triggered image-guided drug delivery," *European Journal of Radiology*, vol. 70, no. 2, pp. 242–253, 2009.

[8] J. R. Lindner, "Molecular imaging of cardiovascular disease with contrast-enhanced ultrasonography," *Nat Rev Cardiol*, vol. 6, no. 7, pp. 475–481, 2009.

[9] R. Deckers and C. T. Moonen, "Ultrasound triggered, image guided, local drug delivery," *Journal of Controlled Release*, vol. 148, no. 1, pp. 25–33, 2010.

[10] M. Afadzi, S. Strand, E. Nilssen, S.-E. Masoy, T. Johansen, R. Hansen, B. Angelsen, and C. de L Davies, "Mechanisms of the ultrasound-mediated intracellular delivery of liposomes and dextrans," *Ultrasonics, Ferroelectrics and Frequency Control, IEEE Transactions on*, vol. 60, no. 1, pp. 21–33, 2013.

[11] Y. Liu, H. Miyoshi, and M. Nakamura, "Encapsulated ultrasound microbubbles: therapeutic application in drug/gene delivery." *J Control Release*, vol. 114, no. 1, pp. 89–99, 2006.

[12] A. van Wamel, K. Kooiman, M. Harteveld, M. Emmer, F. J. ten Cate, M. Versluis, and N. de Jong, "Vibrating microbubbles poking individual cells: Drug transfer into cells via sonoporation," *Journal of Controlled Release*, vol. 112, no. 2, pp. 149–155, 2006.

[13] J. L. Bull, "The application of microbubbles for targeted drug delivery," *Expert Opin. Drug Deliv.*, vol. 4, no. 5, pp. 475–493, Sep. 2007.

[14] K. Ferrara, R. Pollard, and M. Borden, "Ultrasound microbubble contrast agents: Fundamentals and application to gene and drug delivery," *Annu. Rev. Biomed. Eng.*, vol. 9, no. 1, pp. 415–447, 2007.

[15] A. Rahim, S. L. Taylor, N. L. Bush, G. R. ter Haar, J. C. Bamber, and C. D. Porter, "Physical parameters affecting ultrasound/microbubble-mediated gene delivery efficiency in vitro," *Ultrasound in Medicine & Biology*, vol. 32, no. 8, pp. 1269–1279, 2006.

[16] L. C. Phillips, A. L. Klibanov, B. R. Wamhoff, and J. A. Hossack, "Targeted gene transfection from microbubbles into vascular smooth muscle cells using focused, ultrasound-mediated delivery," *Ultrasound in Medicine & Biology*, vol. 36, no. 9, pp. 1470–1480, 2010.

[17] J. L. Tlaxca, J. J. Rychak, P. B. Ernst, P. R. Konkalmatt, T. I. Shevchenko, T. T. Pizzaro, J. Rivera-Nieves, A. L. Klibanov, and M. B. Lawrence, "Ultrasound-based molecular imaging and specific gene delivery to mesenteric vasculature by endothelial adhesion molecule targeted microbubbles in a mouse model of crohn's disease," *Journal of Controlled Release*, vol. 165, no. 3, pp. 216–225, Feb. 2013.

[18] S. Chang, J. Guo, J. Sun, S. Zhu, Y. Yan, Y. Zhu, M. Li, Z. Wang, and R. X. Xu, "Targeted microbubbles for ultrasound mediated gene transfection and apoptosis induction in ovarian cancer cells," *Ultrasonics Sonochemistry*, vol. 20, no. 1, pp. 171–179, 2013.

[19] J. Escoffre, A. Novell, J. Piron, A. Zeghimi, A. Doinikov, and A. Bouakaz, "Microbubble attenuation and destruction: are they involved in sonoporation efficiency?" *Ultrasonics, Ferroelectrics and Frequency Control, IEEE Transactions on*, vol. 60, no. 1, pp. 46–52, 2013.

[20] E. P. Stride and C. C. Coussios, "Cavitation and contrast: the use of bubbles in ultrasound imaging and therapy," *Proceedings of the Institution of Mechanical Engineers, Part H: Journal of Engineering in Medicine*, vol. 224, no. 2, pp. 171–191, 2010.

[21] A. Alzaraa, G. Gravante, W. Y. Chung, D. Al-Leswas, M. Bruno, A. R. Dennison, and D. M. Lloyd, "Targeted microbubbles in the experimental and clinical setting," *The American Journal of Surgery*, vol. 204, no. 3, pp. 355–366, Sep. 2012.

[22] W. J. Greenleaf, M. E. Bolander, G. Sarkar, M. B. Goldring, and J. F. Greenleaf, "Artificial cavitation nuclei significantly enhance acoustically induced cell transfection," *Ultrasound in Medicine & Biology*, vol. 24, no. 4, pp. 587–595, 1998.

[23] A. Delalande, S. Kotopoulis, M. Postema, P. Midoux, and C. Pichon, "Sonoporation: Mechanistic insights and ongoing challenges for gene transfer," *Gene*, p. In Press, 2013.

[24] A. A. Doinikov and A. Bouakaz, "Theoretical investigation of shear stress generated by a contrast microbubble on the cell membrane as a mechanism for sonoporation," *J. Acoust. Soc. Am.*, vol. 128, no. 1, pp. 11–19, 2010.

[25] A. Delalande, S. Kotopoulis, T. Rovers, C. Pichon, and M. Postema, "Sonoporation at a low mechanical index," *Bubble Science, Engineering & Technology*, vol. 3, no. 1, pp. 3–12, 2011.

[26] J. Wu, J. P. Ross, and J.-F. Chiu, "Reparable sonoporation generated by microstreaming," *J. Acoust. Soc. Am.*, vol. 111, no. 3, pp. 1460–1464, Mar. 2002.

[27] P. Prentice, A. Cuschieri, K. Dholakia, M. Prausnitz, and P. Campbell, "Membrane disruption by optically controlled microbubble cavitation," *Nat Phys*, vol. 1, no. 2, pp. 107–110, 2005.

[28] M. M. Forbes, R. L. Steinberg, and W. D. O'Brien Jr., "Examination of inertial cavitation of optison in producing sonoporation of chinese hamster ovary cells," *Ultrasound in Medicine & Biology*, vol. 34, no. 12, pp. 2009–2018, 2008.

[29] B. Geers, I. Lentacker, N. N. Sanders, J. Demeester, S. Meairs, and S. C. De Smedt, "Self-assembled liposome-loaded microbubbles: The missing link for safe and efficient ultrasound triggered drug-delivery," *Journal of Controlled Release*, vol. 152, no. 2, pp. 249–256, 2011.

[30] J. Escoffre, C. Mannaris, B. Geers, A. Novell, I. Lentacker, M. Averkiou, and A. Bouakaz, "Doxorubicin liposome-loaded microbubbles for contrast imaging and ultrasound-triggered drug delivery," *Ultrasonics, Ferroelectrics and Frequency Control, IEEE Transactions on*, vol. 60, no. 1, pp. 78–87, 2013.

[31] K. Hettiarachchi, E. Talu, M. L. Longo, P. A. Dayton, and A. P. Lee, "On-chip generation of microbubbles as a practical technology for manufacturing contrast agents for ultrasonic imaging," *Lab Chip*, vol. 7, no. 4, pp. 463–468, 2007.

[32] A. Dhanaliwala, J. Chen, S. Wang, and J. Hossack, "Liquid flooded flow-focusing microfluidic device for in situ generation of monodisperse microbubbles," *Microfluidics and Nanofluidics*, pp. 1–11, 2012.

[33] S. A. Peyman, R. H. Abou-Saleh, J. R. McLaughlan, N. Ingram, B. R. G. Johnson, K. Critchley, S. Freear, J. A. Evans, A. F. Markham, P. L. Coletta, and S. D. Evans, "Expanding 3d geometry for enhanced on-chip

microbubble production and single step formation of liposome modified microbubbles," *Lab Chip*, vol. 12, no. 21, pp. 4544–4552, 2012.
[34] Y. Liu, J. Yan, and M. R. Prausnitz, "Can ultrasound enable efficient intracellular uptake of molecules? a retrospective literature review and analysis," *Ultrasound in Medicine & Biology*, vol. 38, no. 5, pp. 876–888, 2012.
[35] R. E. Apfel and C. K. Holland, "Gauging the likelihood of cavitation from short-pulse, low-duty cycle diagnostic ultrasound," *Ultrasound in Medicine & Biology*, vol. 17, no. 2, pp. 179–185, 1991.
[36] C. C. Church, "Frequency, pulse length, and the mechanical index," *ARLO*, vol. 6, no. 3, pp. 162–168, 2005.
[37] K. Morgan, J. Allen, P. Dayton, J. Chomas, A. Klibaov, and K. Ferrara, "Experimental and theoretical evaluation of microbubble behavior: effect of transmitted phase and bubble size," *Ultrasonics, Ferroelectrics and Frequency Control, IEEE Transactions on*, vol. 47, no. 6, pp. 1494–1509, 2000.
[38] R. Chiao and X. Hao, "Coded excitation for diagnostic ultrasound: a system developer's perspective," in *Ultrasonics, 2003 IEEE Symposium on*, vol. 1, 2003, pp. 437–448 Vol.1.
[39] D. Cowell and S. Freear, "Separation of overlapping linear frequency modulated (LFM) signals using the fractional Fourier transform," *Ultrasonics, Ferroelectrics and Frequency Control, IEEE Transactions on*, vol. 57, no. 10, pp. 2324–2333, 2010.
[40] G. T. Clement, H. Nomura, and T. Kamakura, "The feasibility of pulse compression by nonlinear effective bandwidth extension," *J. Acoust. Soc. Am.*, vol. 130, no. 4, pp. 1810–1819, 2011.
[41] J. Borsboom, C. T. Chin, A. Bouakaz, M. Versluis, and N. de Jong, "Harmonic chirp imaging method for ultrasound contrast agent," *Ultrasonics, Ferroelectrics and Frequency Control, IEEE Transactions on*, vol. 52, no. 2, pp. 241–249, 2005.
[42] Y. Sun, D. Kruse, and K. Ferrara, "Contrast imaging with chirped excitation," *Ultrasonics, Ferroelectrics and Frequency Control, IEEE Transactions on*, vol. 54, no. 3, pp. 520–529, 2007.
[43] J. M. Borsboom, C. T. Chin, and N. de Jong, "Nonlinear coded excitation method for ultrasound contrast imaging," *Ultrasound in Medicine & Biology*, vol. 29, no. 2, pp. 277–284, 2003.
[44] P. J. Frinking, I. Tardy, M. Thraulaz, M. Arditi, J. Powers, S. Pochon, and F. Tranquart, "Effects of acoustic radiation force on the binding efficiency of br55, a vegfr2-specific ultrasound contrast agent," *Ultrasound in Medicine & Biology*, vol. 38, no. 8, pp. 1460–1469, 2012.
[45] T. G. Leighton, *The Acoustic Bubble*. Academic Press, 1994.
[46] P. Dayton, K. Morgan, A. Klibanov, G. Brandenburger, K. Nightingale, and K. Ferrara, "A preliminary evaluation of the effects of primary and secondary radiation forces on acoustic contrast agents," *Ultrasonics, Ferroelectrics and Frequency Control, IEEE Transactions on*, vol. 44, no. 6, pp. 1264–1277, 1997.
[47] P. Dayton, A. Klibanov, G. Brandenburger, and K. Ferrara, "Acoustic radiation force in vivo: a mechanism to assist targeting of microbubbles," *Ultrasound in Medicine & Biology*, vol. 25, no. 8, pp. 1195–1201, 1999.
[48] P. A. Dayton, J. S. Allen, and K. W. Ferrara, "The magnitude of radiation force on ultrasound contrast agents," *J. Acoust. Soc. Am.*, vol. 112, no. 5, pp. 2183–2192, 2002.
[49] A. A. Doinikov and S. T. Zavtrak, "On the "bubble grapes" induced by a sound field," *J. Acoust. Soc. Am.*, vol. 99, no. 6, pp. 3849–3850, 1996.
[50] Y. Hu, D. Zhang, H. Zheng, and X. Gong, "Chirp excitation technique to enhance microbubble displacement induced by ultrasound radiation force," *J. Acoust. Soc. Am.*, vol. 125, no. 3, pp. 1410–1415, 2009.
[51] J. McLaughlan, P. Smith, N. Ingram, L. Coletta, S. Evans, and S. Freear, "Chirp excitation of polydisperse microbubble populations for increasing sonoporation efficiency," in *Ultrasonics, 2012 IEEE Symposium on*, 2012, pp. 2298–2301.
[52] D. Chatterjee, P. Jain, and K. Sarkar, "Ultrasound-mediated destruction of contrast microbubbles used for medical imaging and drug delivery," *Phys. Fluids*, vol. 17, no. 10, pp. 100 603–100 608, Oct. 2005.
[53] C. E. Brennen, *Cavitation and Bubble Dynamics*. Oxford University Press, 1995.
[54] D. Goertz, M. Frijlink, A. Bouakaz, C. Chin, N. de Jong, and A. van der Steen, "The effects of bubble size on nonlinear scattering from microbubbles," in *Ultrasonics, 2003 IEEE Symposium on*, vol. 2, 2003, pp. 1503–1506.
[55] D. E. Goertz, N. de Jong, and A. F. van der Steen, "Attenuation and size distribution measurements of definity and manipulated definity populations," *Ultrasound in Medicine & Biology*, vol. 33, no. 9, pp. 1376–1388, 2007.
[56] T. Faez, D. Goertz, and N. De Jong, "Characterization of definity ultrasound contrast agent at frequency range of 515 mhz," *Ultrasound in Medicine & Biology*, vol. 37, no. 2, pp. 338–342, 2011.
[57] P. R. Smith, D. M. J. Cowell, B. Raiton, C. V. Ky, and S. Freear, "Ultrasound array transmitter architecture with high timing resolution using embedded phase-locked loops," *Ultrasonics, Ferroelectrics and Frequency Control, IEEE Transactions on*, vol. 59, no. 1, pp. 40–49, 2012.
[58] P. Smith, D. Cowell, and S. Freear, "Width-modulated square-wave pulses for ultrasound applications," *Ultrasonics, Ferroelectrics and Frequency Control, IEEE Transactions on*, p. In press, 2012.
[59] S. Lavilla-Alonso, G. Bauerschmitz, U. Abo-Ramadan, J. Halavaara, S. Escutenaire, I. Diaconu, T. Tatlisumak, A. Kanerva, A. Hemminki, and S. Pesonen, "Adenoviruses with an ?v? integrin targeting moiety in the fiber shaft or the hi-loop increase tumor specificity without compromising antitumor efficacy in magnetic resonance imaging of colorectal cancer metastases," *Journal of Translational Medicine*, vol. 8:80, pp. 1–11, 2010.
[60] W. S. Kamoun, S.-S. Chae, D. A. Lacorre, J. A. Tyrrell, M. Mitre, M. A. Gillissen, D. Fukumura, R. K. Jain, and L. L. Munn, "Simultaneous measurement of rbc velocity, flux, hematocrit and shear rate in vascular networks," *Nat Meth*, vol. 7, no. 8, pp. 655–660, Aug. 2010.
[61] M. Kinoshita and K. Hynynen, "Intracellular delivery of bak bh3 peptide by microbubble-enhanced ultrasound," *Pharmaceutical Research*, vol. 22, no. 5, pp. 716–720, 2005.
[62] R. Karshafian, S. Samac, P. D. Bevan, and P. N. Burns, "Microbubble mediated sonoporation of cells in suspension: Clonogenic viability and influence of molecular size on uptake," *Ultrasonics*, vol. 50, no. 7, pp. 691–697, 2010.
[63] S. Wong, M. Kupnik, R. Watkins, K. Butts-Pauly, and B. Khuri-Yakub, "Capacitive micromachined ultrasonic transducers for therapeutic ultrasound applications," *Biomedical Engineering, IEEE Transactions on*, vol. 57, no. 1, pp. 114–123, 2010.
[64] H. Pan, Y. Zhou, O. Izadnegahdar, J. Cui, and C. X. Deng, "Study of sonoporation dynamics affected by ultrasound duty cycle," *Ultrasound in Medicine & Biology*, vol. 31, no. 6, pp. 849–856, Jun. 2005.
[65] B. J. Schmidt, I. Sousa, A. A. van Beek, and M. R. Bhmer, "Adhesion and ultrasound-induced delivery from monodisperse microbubbles in a parallel plate flow cell," *Journal of Controlled Release*, vol. 131, no. 1, pp. 19–26, 2008.
[66] V. Garbin, M. Overvelde, B. Dollet, N. de Jong, D. Lohse, and M. Versluis, "Unbinding of targeted ultrasound contrast agent microbubbles by secondary acoustic forces," *Physics in Medicine and Biology*, vol. 56, no. 19, pp. 6161–6177, 2011.
[67] K. Kooiman, M. Foppen-Harteveld, A. F. v. der Steen, and N. de Jong, "Sonoporation of endothelial cells by vibrating targeted microbubbles," *Journal of Controlled Release*, vol. 154, no. 1, pp. 35–41, 2011.
[68] A. L. Klibanov, P. T. Rasche, M. S. Hughes, J. K. Wojdyla, K. P. Galen, J. H. J. Wible, and G. H. Brandenburger, "Detection of individual microbubbles of ultrasound contrast agents: Imaging of free-floating and targeted bubbles," *Investigative Radiology*, vol. 39, no. 3, pp. –, 2004.

James McLaughlan received his M.Phys. degree in Physics from the University of Bath in 2004, and gained his PhD in 2008 working on the optimisation of high intensity focused ultrasound therapy with cavitation at the Institute of Cancer Research. Subsequently, he moved to Boston University as a post-doctoral research associate where he investigated the use of optical contrast agents exposed to light and sound for the nucleation of cavitation for imaging and therapeutic applications. In 2010 he joined the Ultrasound Group within the School of Electronic and Electrical Engineering at the University of Leeds where he is part of a multidisciplinary team working on engineering therapeutic microbubbles for colorectal cancer treatment. Within the same group he is about to start as an early career research fellow studying the use of nanoparticles for breast cancer imaging and therapy.

Nicola Ingram gained her PhD in 2004 working on gene therapy methods targeting tumour vasculature at the Institute of Cancer Research. Subsequently, she moved to the University of Leeds to work on gene therapy for ovarian cancer and later on mouse models in colorectal cancer. At present she is a part of a multidisciplinary team working on therapeutic microbubbles for colorectal cancer treatment and her current interests are in drug/gene delivery to cancer and in vivo imaging.

Peter Smith received his B.Eng. (Hons) degree in Electronic Engineering (Industrial) and a M.Sc. degree in Embedded Systems Engineering from the University of Leeds, UK, in 2008 and 2009 respectively. As part of his undergraduate studies he completed a 12 month industrial placement working within Hardware Design Verification. His postgraduate M.Sc. project was the design of an 8-Channel FPGA-controlled Ultrasound Transmitter design. In 2009 he joined the Ultrasound Group within the School of Electronic and Electrical Engineering as a Ph.D. student. His main research interests include ultrasound instrumentation and system design, FPGA development, and ultrasound medical imaging.

Sevan Harput received the B.Sc. degree in Microelectronics Engineering and the M.Sc. in Electronic Engineering and Computer Sciences from Sabancı University, Turkey in 2005 and 2007, respectively. He received the Ph.D. degree in 2012 from the University of Leeds. He worked as a teaching and research fellow in Sabancı University between 2007 and 2008. In 2009, he joined to the Ultrasound Group in the School of Electronic and Electrical Engineering, University of Leeds. Currently, he is working as a research fellow in the University of Leeds and he is an administrative assistant in the IEEE Transactions on Ultrasonics, Ferroelectrics and Frequency Control. His research interests include ultrasound medical imaging, coded excitation, nonlinear acoustics and ultrasound contrast agents.

P. Louise Coletta leads the Pre-clinical Translation and Imaging Group at the Leeds Institute of Molecular Medicine. Her interest lies in understanding the mechanisms that drive colorectal cancer progression and identification of novel therapeutic targets. She is also a member of the Leeds Microbubble Consortium and works closely with the multidisciplinary team engaged in the development of therapeutic microbubbles for the treatment of cancer.

Stephen Evans obtained his B.Sc. in Physics from the University of London (QMC) in 1984 and his PhD in Molecular Physics from the University of Lancaster in 1988. After a post-doctoral fellowship at Imperial College, University of London, he became a visiting scientist in the Molecular and Optical Electronic Research Laboratory, Eastman Kodak, Rochester, New York. He joined the academic staff of the University of Leeds in 1991, became a Reader in 2001, and was appointed as Professor in Molecular Physics and Nanoscale Physics in 2002. He was Chairman of the School of Physics & Astronomy between 2004-2007 and currently heads the Molecular and Nanoscale Physics group.

Steven Freear (S'95, M'97, SM'11) gained his doctorate in 1997 and subsequently worked in the electronics industry for 7 years as a medical ultrasonic system designer. He was appointed Lecturer (Assistant Professor) and then Senior Lecturer (Associate Professor) in 2006 and 2008 respectively at the School of Electronic and Electrical Engineering at the University of Leeds. In 2006 he formed the Ultrasound Group specializing in both industrial and biomedical research. His main research interest is concerned with advanced analogue and digital signal processing and instrumentation for ultrasonic systems. He teaches digital signal processing, VLSI and embedded systems design, and hardware description languages at both undergraduate and postgraduate level. He has been Associate Editor for IEEE Transactions on Ultrasonics, Ferrorelectrics and Frequency Control since 2009, and was appointed Editor-In-Chief in 2013.